

# Left-Handed Material Inspired Multi-Layer Planar Antenna Design for Satellite Communication Applications

Trushit Upadhyaya<sup>1, \*</sup>, Rajat Pandey<sup>1</sup>, Upesh Patel<sup>1</sup>, Killol Pandya<sup>1</sup>, Arpan Desai<sup>1</sup>, Riki Patel<sup>2</sup>, and Yogeshwar Kosta<sup>1</sup>

**Abstract**—Investigations on radiation characteristics of multilayer antenna having embedment of left-handed material are presented. The proposed engineered comb-shaped structure exhibits both negative permittivity and permeability. The inset-fed patch antenna matched at  $50\ \Omega$  incorporates a homogeneous array of multilayer comb-shaped resonators. The array demonstrates a major impact on antenna parameters such as resonance, gain, radiation pattern, voltage standing wave ratio, and bandwidth. The novelty in the presented design is that by merely modifying the physical parameters of the negative refractive index resonator, the antenna radiation property can be altered. An artificially realized left-handed stacked material possesses strong inductive and capacitive mutual-coupling. The variations in stacked conductive inclusion illustrate the considerable change in antenna resonance. The antenna resonates at 1.57 GHz, 2.48 GHz, and 3.4 GHz with a bandwidth of around 20.64%, 7.35%, and 4.40% respectively. The proposed antenna electrical size is  $0.48\lambda \times 0.56\lambda$  at a lower frequency. The antenna exhibits the gain of 3.8 dBi, 6.15 dBi, 4.54 dBi at 1.57 GHz, 2.48 GHz, and 3.4 GHz, respectively. The proposed planar stacked negative refractive index-inspired patch antenna model can be utilized for L1 and S-band satellite and maritime operations.

## 1. INTRODUCTION

Microstrip patch antenna is one of the widely utilized printed antennas for satellite applications due to its surface-mountable structure, low cost, and low design complexities. Recent developments in artificial dielectric materials, also known as left-handed materials, have created a significant impact on advanced antennas and microwave components design. Since the inception of the metamaterial concepts given by Veselago, verified by Pendry, and experimentally proven by Smith et al., the developments in negative refraction inspired technology is immense [1, 2]. Scientists across the globe have experimentally achieved the benefits of left-handed material for practical applications.

Nature has given negative materials. Gold and silver possess negative permittivity ( $\epsilon$ ) whereas ferromagnetic and anti-ferromagnetic materials possess negative permeability ( $\mu$ ). However, the realization of simultaneous negative permittivity ( $\epsilon$ ) and permeability ( $\mu$ ) using conducting thin wire and split ring resonators (SRRs) provided a revolution in the microwave and wireless communication community. The engineered materials have shown highly impressive growth, which has inspired a resurgence of innovative creations in the design of novel negative refractive index material. The size of metamaterial elements needs to be comparable to their wavelength, typically in the range of  $\lambda/10$  or lesser. The sub-wavelength dimensions utilized in the homogenous array pattern improve the electric and magnetic properties of the host material, especially in the antenna design. The physics and experimental realization of negative refractive index material are adequately discussed in [3, 4]. The refraction indices

---

*Received 12 December 2021, Accepted 15 February 2022, Scheduled 26 February 2022*

\* Corresponding author: Trushit Upadhyaya (trushitupadhyaya.ec@charusat.ac.in).

<sup>1</sup> Department of Electronics and Communication Engineering, Chandubhai S. Patel Institute of Technology, Charotar University of Science and Technology (CHARUSAT), Changa 388421, India. <sup>2</sup> Florida Atlantic University, Florida, USA.

provide the measure of deflection which an electromagnetic wave undergoes at the material interface. Left-handed materials (LHMs) are variably coupled with microwave active and passive devices especially antennas for a range of applications. The lenses formed by the engineered artificial material aid in antenna designs.

Several types of metamaterials inspired antennas are envisaged, theoretically analyzed, simulated, and fabricated to date for real-time applications such as compact and miniaturized antennas [5–8], Broadband Antennas [9–11], Beam tilting Antennas [12, 13], Antennas for MIMO Applications [14, 15], Ultra-wideband Applications Antennas [16, 17], and Transparent Antennas [18, 19]. The metamaterial-inspired antennas can have different configurations such as multilayer [20, 21], etched in the ground plane [22], or radome [23, 24] to exploit the benefits of left-handed materials. The radome resonance is due to propagating eigenmodes of conducting metallic array, and such design considerably improves the directivity of the antenna. There is also the availability of both near-field [25, 26] and far-field [27, 28] application-specific antennas in literature. The left-handed material loading may be symmetrical or asymmetrical depending on applications; however, significant improvements have been achieved compared to conventional half-wavelength or full wavelength printed antennas. This paper explores the utilization of negative refractive index material-loaded bilayered substrate.

## 2. NEGATIVE REFRACTION ANALYSIS

If the material is having a single propagating mode for a specific resonance frequency, then the material will possess a well-specified refractive index irrespective of homogenous or heterogeneous nature. The comb structure unit cell was simulated by keeping E-field oriented in a vertical direction interacting with the face of comb and  $k$ -vector moving along the comb.

The following equation shows impedance parameters [20]

$$A = \frac{Z_{11}}{Z_{21}}, \quad B = \frac{Z_{11}Z_{22} - Z_{21}^2}{Z_{21}}, \quad C = \frac{1}{Z_{21}}, \quad D = \frac{Z_{22}}{Z_{21}} \quad (1)$$

The complex propagation constant ( $\gamma$ ) in the form of impedance parameters can be given as:

$$\gamma = \frac{\operatorname{arccosh} \left( \frac{A + D}{2} \right)}{a_x} \quad (2)$$

The Bloch impedance in terms of impedance parameters can be shown as:

$$Z_B = \frac{Be^{-\gamma d}}{1 - Ae^{-\gamma d}} \quad (3)$$

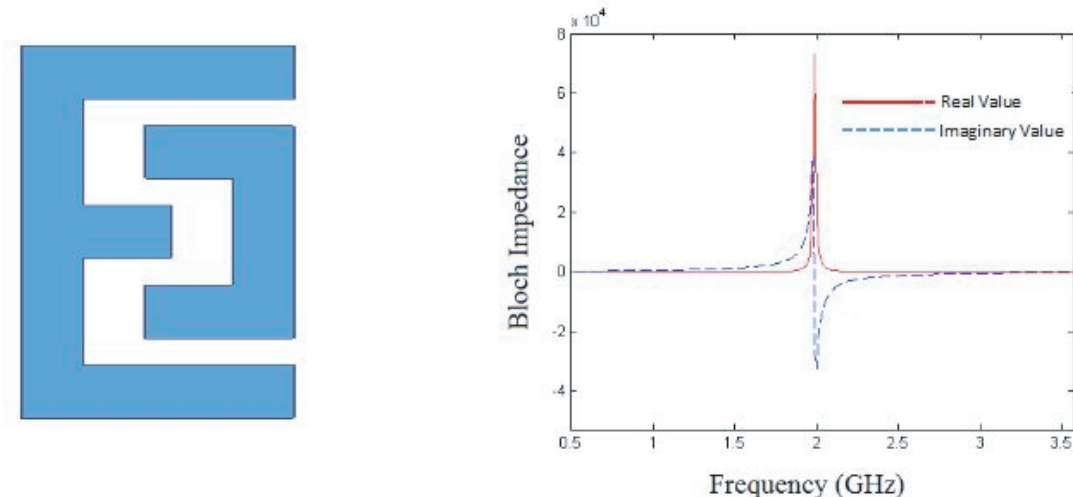


**Figure 1.** Comb resonator and Bloch Impedance.

The calculated Bloch impedance for the comb-shaped resonator is illustrated in Fig. 1. The propagation constant can be shown in terms of attenuation ( $\alpha$ ) and phase constants ( $\beta$ )

$$\gamma = \alpha + j\beta \tag{4}$$

The effective relative permittivity ( $\epsilon_{reff}$ ) and effective relative permeability ( $\mu_{reff}$ ) are given by

$$\mu_{reff} = \frac{-j\gamma Z_B}{Z_{line} k_0}, \quad \epsilon_{reff} = \frac{-j\gamma Z_{line}}{Z_B k_0} \tag{5}$$

$k_0$ : free space wavenumber;  $Z_{line}$ : line impedance;  $ax$ ,  $ay$ , and  $az$ : unit cell dimensions.

There are numerous techniques available to calculate the refractive index of the material. The effective parameters retrieval technique demonstrated in [20] was utilized to calculate  $\epsilon_{reff}$  and  $\mu_{reff}$  as shown in Fig. 2, which confirms that comb structure exhibits double negative (DNG) refraction behavior.

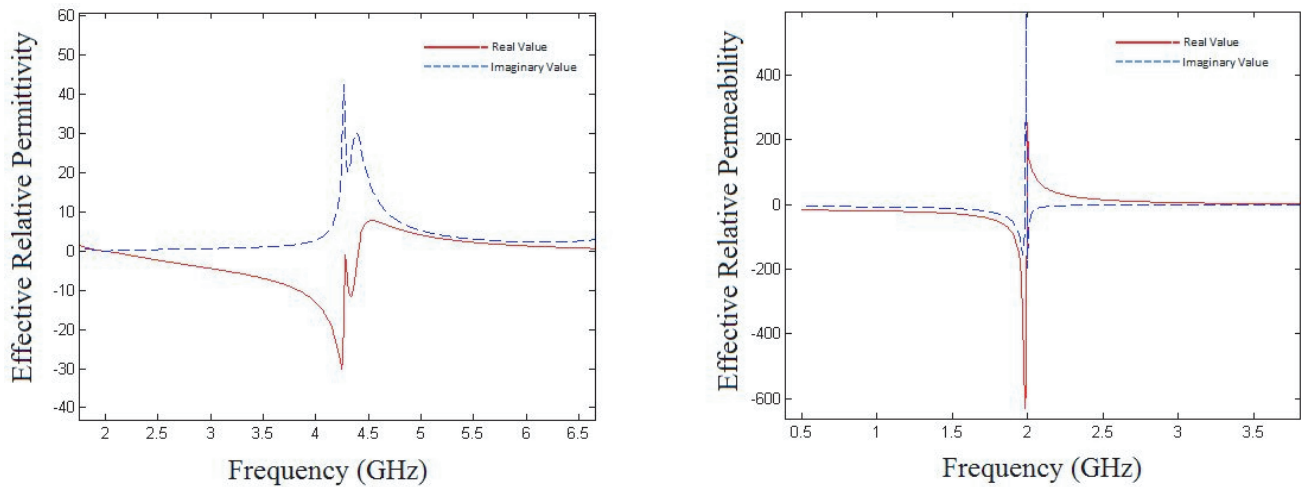


**Figure 2.** Effective Permittivity and Permeability of comb resonator.

### 3. PROPOSED SATELLITE COMMUNICATION ANTENNA DESIGN

The proposed double negative material-inspired resonator and geometric dimensions parameters are illustrated in Fig. 3. At lower frequency, patch dimension is  $0.36\lambda \times 0.40\lambda$ , and ground plane dimension is  $0.48\lambda \times 0.56\lambda$ . Total substrate thickness ( $h_s$ ) is 60 mil having three layers of 20 mils Arlon AD255 material. The AD255 material is a low-loss material having a dielectric constant of 2.5. The dielectric loss tangent of AD 255 material is 0.0014 which makes it suitable for high-frequency antenna design. The dielectric losses increase at very high frequencies for the material whose loss tangent is high. The metallic inclusion is sandwiched between three layers of a thin AD255 substrate. The inclusion of comb metal in the substrate makes the antenna a metamaterial-inspired resonator. The presence of negative refractive index material in the substrate further decreases the effective dielectric constant. The metallic inclusion reduces the dielectric losses, and hence the antenna becomes useful at high-frequency operations. The antenna resonance is controlled by tailoring dimensions, placement, and orientation of patch and metallic inclusion.

The symmetrical slotted patch resonator loaded with an array of  $3 \times 2$  comb metallic inclusion and geometry parameters are depicted in Fig. 3. The antenna is inset-fed which is matched at  $50\Omega$ . Tuning slots are provided for fine-tuning of the antenna at the desired frequency; however, presented results utilize the tuning capability primarily of metallic inclusions. The analysis in the variation in geometrical parameters of comb structure is carried out to illustrate that the antenna can be tuned by modifying comb resonator dimensions as illustrated in Fig. 4. As the dimensions of the comb structure strips are varied, the equivalent inductance and capacitance change respectively.

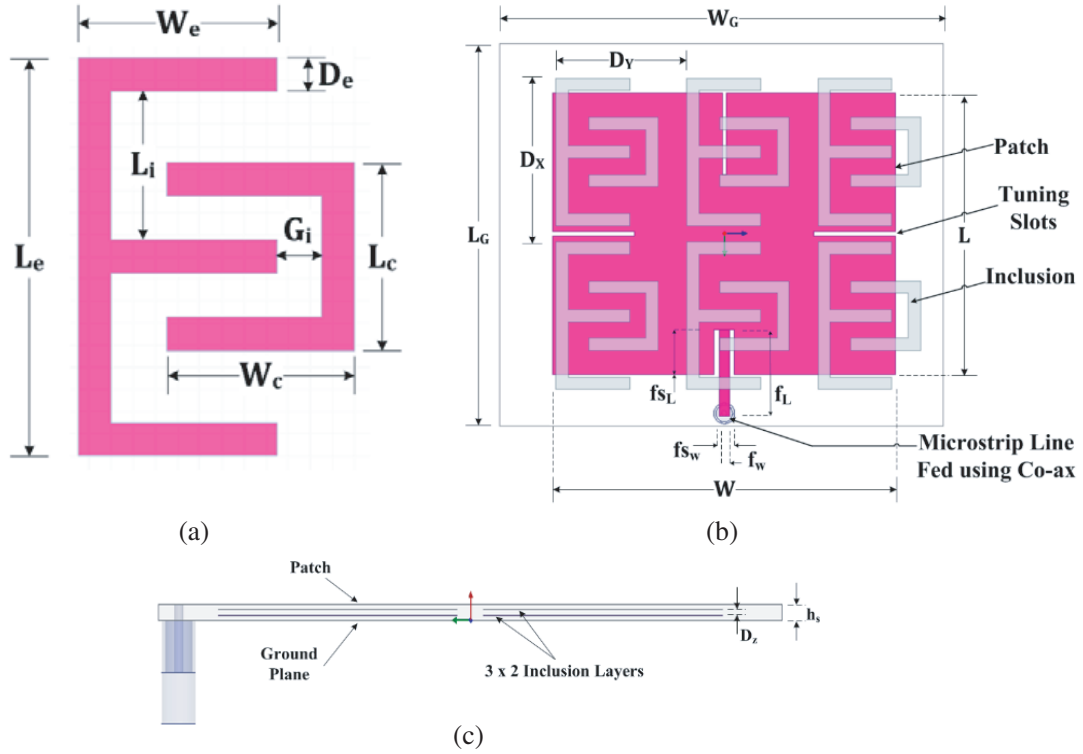


**Figure 3.** Antenna geometry. (a) Unit cell design. (b) Top orientation. (c) Side orientation.

The strong magnetic coupling between comb resonators decreases with further increment in the distance. In addition, coupling inductance and capacitance would also get varied significantly between elements of comb-shaped resonator array; however, the variations in dielectric material capacitance will

**Table 1.** Antenna design parameters.

Notation	Dimension (mm)
$L$	69
$W$	78
$W_G$	92
$L_G$	107
$L_e$	34
$W_e$	16
$D_e$	3
$L_c$	16
$f_L$	20
$D_c$	3
$L_i$	12.6
$G_i$	6
$D_x$	38
$D_y$	30
$D_z$	1.56
$f_W$	2.5
$W_c$	16

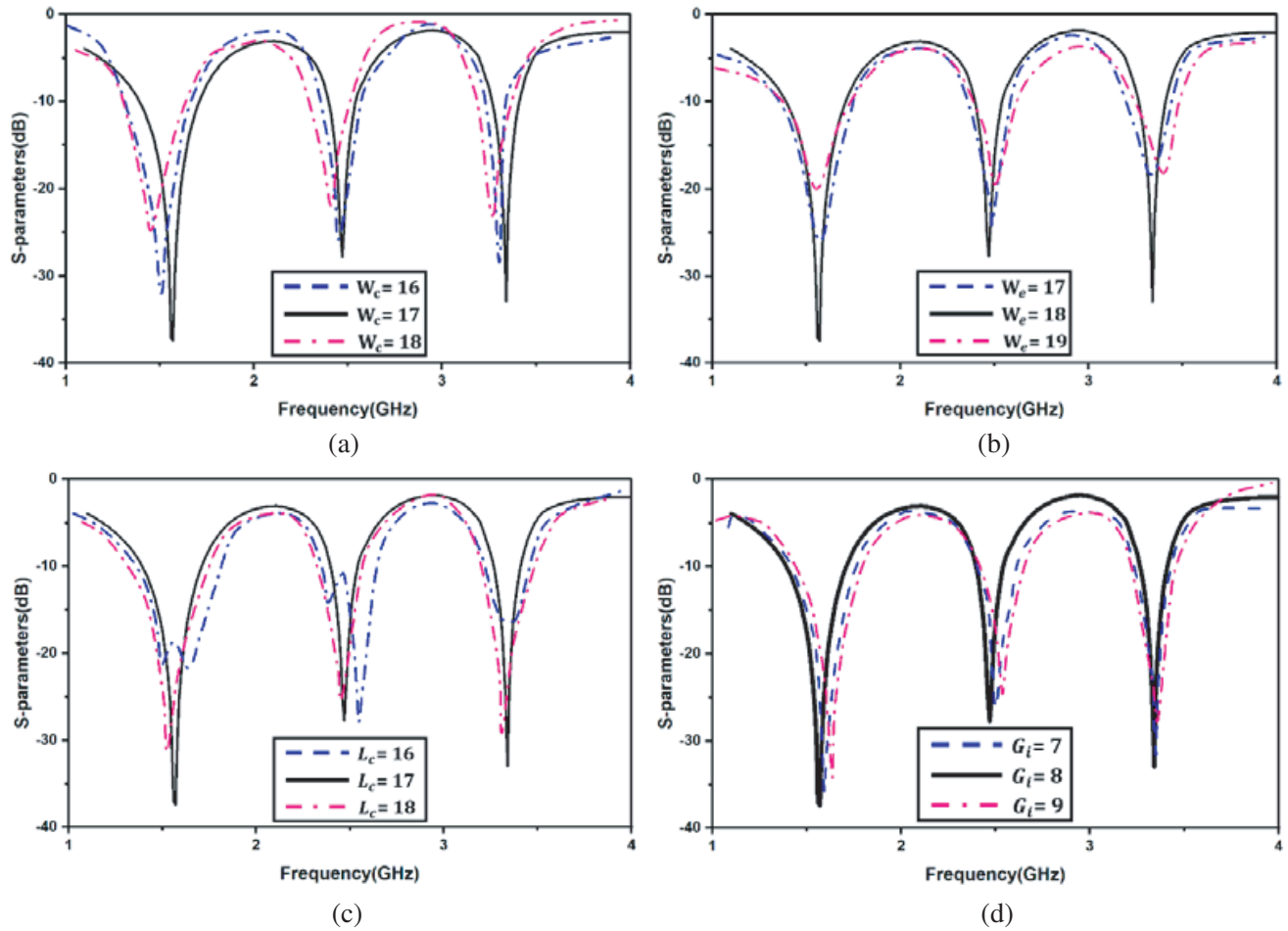


**Figure 4.** Effect of parametric variation on reflection coefficient. (a)  $W_c$ . (b)  $W_e$ . (c)  $L_c$ . (d)  $G_i$ .

be quite low, and it can be neglected in antenna tuning. The effective mutual capacitance and mutual inductance decrease as the distance between comb-shaped resonators increases. These figures illustrate that mere modification in comb resonator leads to desired frequency operation in L and S bands.

The close placement of resonators in a  $2 \times 3$  array induces strong magnetic coupling, and output resonance has a significant influence on mutual capacitance and inductance.

The width of tuning slots on the patch is 1 mm to fine-tune the target frequency. Antenna design dimensions are enlisted in Table 1. All antenna geometrical parameters along with comb resonator parameters can be varied for tuning the antenna at the desired bands of operation. The fabricated antenna prototype is illustrated in Fig. 5. The feed is soldered to a  $50 \Omega$  SMA connector.

#### 4. SIMULATION AND MEASUREMENT RESULTS

The simulated results of return loss were carried out in FEM-based commercial antenna design software. The antenna reflection coefficient measurement was carried out using Keysight 9912A VNA. Simulated and measured return losses for matched impedance conditions are depicted in Fig. 6. The simulated and measured results display a good correlation. The antenna resonates in IEEE L1 and S-band at target frequencies of 1.57 GHz, 2.48 GHz, and 3.4 GHz primarily utilized for India Satellite and Maritime Communication. The 1.57 GHz and 2.48 GHz frequencies are allocated bands for Indian GPS Satellite Communication whereas 3.4 GHz is standard maritime communication frequency.

Typically, bandwidth of metamaterial-inspired antennas is less than standard planar antennas

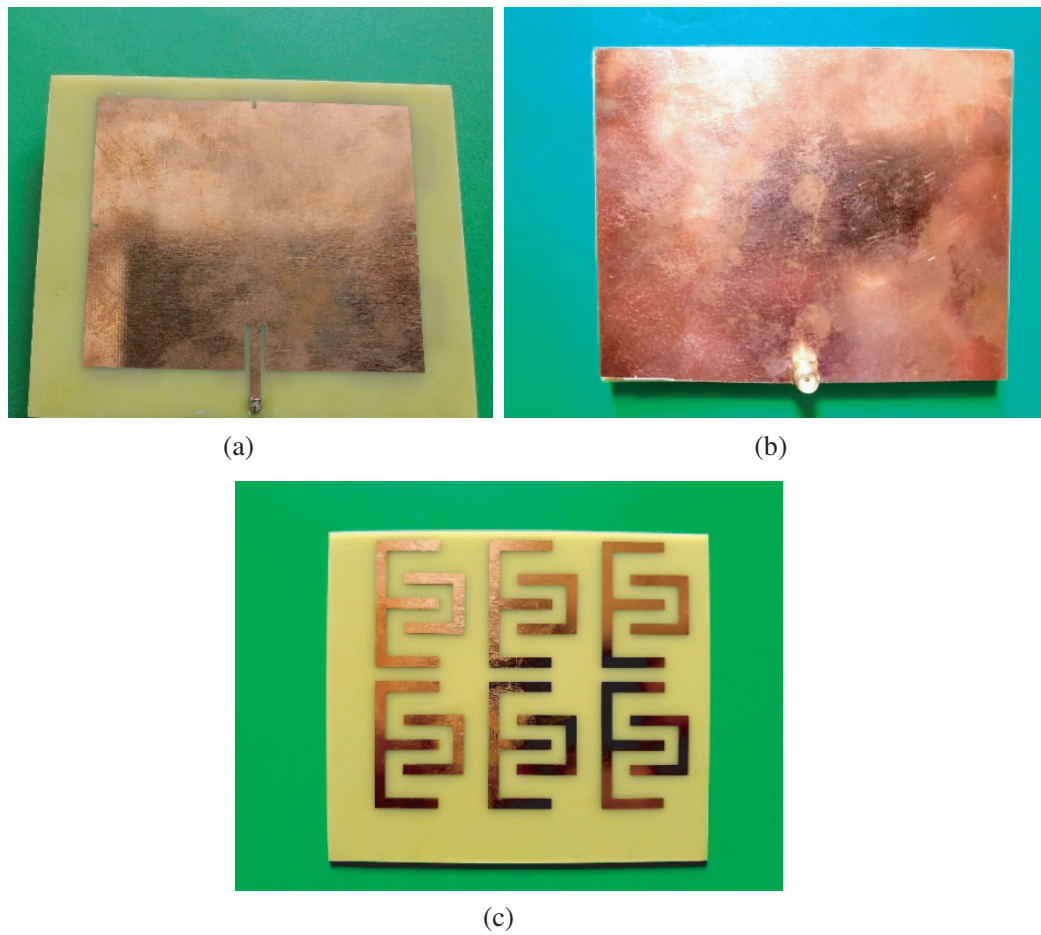


**Figure 5.** Antenna prototype. (a) Top view. (b) Bottom view. (c) Comb layer.

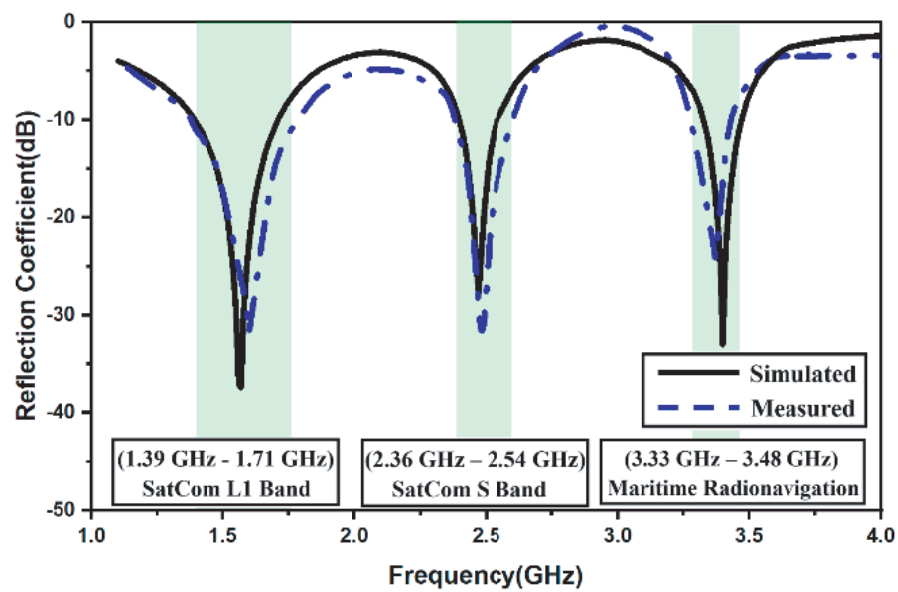


**Figure 6.** Reflection Coefficient of the proposed antenna.

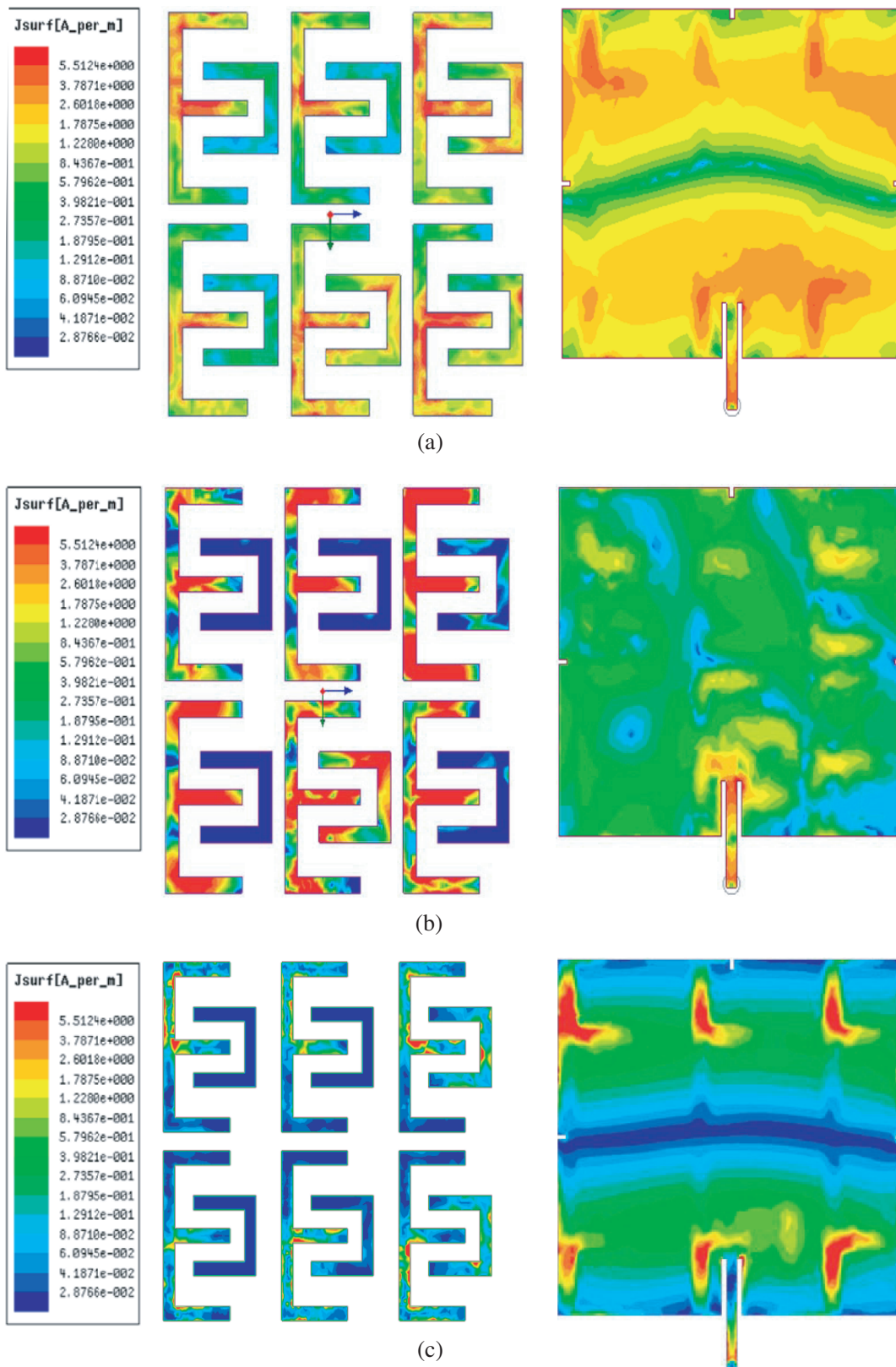


**Figure 7.** Surface current density on middle layer and top layer at target resonances. (a) 1.57 GHz. (b) 2.48 GHz. (c) 3.4 GHz.

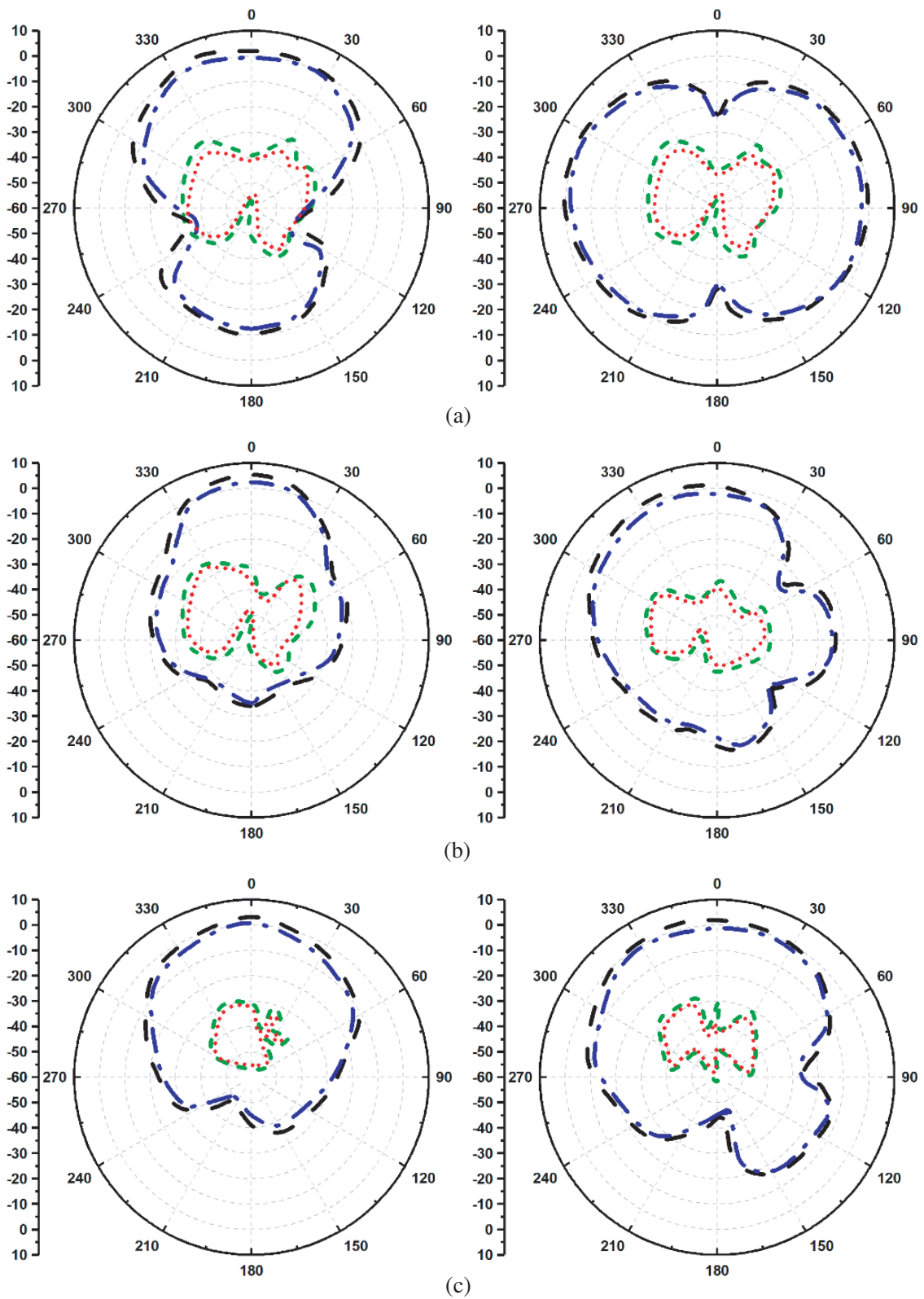


**Figure 8.** Simulated and measured 2D radiation patterns. (a) 1.57 GHz. (b) 2.48 GHz. (c) 3.4 GHz.

because of the high Q-factor of negative refractive index materials and the fundamental limitation of the patch antenna. The proposed design has multiple layers, which causes bandwidth to increase due to the correlation of bandwidth with substrate thickness. The bandwidths of the antenna are 20.64%, 7.35%, and 4.40% at target resonances, respectively.

The current density distributions of comb-shaped resonator and antenna at target frequencies are shown in Fig. 7. The current density on the patch is stronger at the edge of the antenna. As anticipated, the current densities of the resonator at secondary resonances are weak. The radiation patterns of the antenna were experimentally measured in an anechoic chamber environment as depicted in Fig. 8. The antenna peak gain values of 3.8 dBi, 6.15 dBi, and 4.54 dBi were measured for 1.57 GHz, 2.48 GHz, and 3.4 GHz, respectively, which meets the criteria for the target applications.

Figure 9 illustrates the antenna gain and efficiencies at target frequencies. It is apparent from the figure that the antenna meets the desirable gain requirement for space applications. Table 2 illustrates the comparison of the proposed antenna with other antennas for satellite applications. The designed structure is better in terms of number of frequencies and bandwidth where it is under performing in terms of size and gain compared to previously reported literature. The proposed antenna exhibits its usefulness for GPS satellite communication applications.

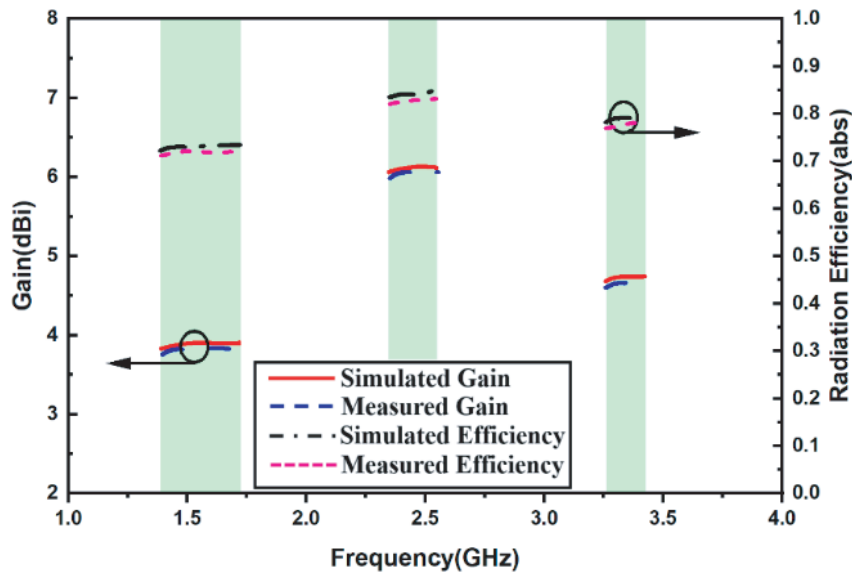


Figure 9. Antenna gain.

Table 2. Performance comparison of the proposed antenna with the existing state of the art antennas.

Reference	Resonance Frequencies	Size (in mm <sup>2</sup> )	Gain (dBi)	BW (%)
[29]	1.2, 1.57	140 × 140	7, 6	2
[30]	2.45, 5.8	58.71 × 58.71	—	6.8
[31]	2.4, 5	69.5 × 10	3-4	2.1, 7.33
[32]	1.5 – 1.65	40 × 40	5	6.25
Proposed	1.57, 2.48, 3.4	90 × 107	3.8, 6.15, 4.54	20.64, 7.35, 4.40

## 5. CONCLUSION

An engineered multilayer left-handed material-inspired resonator is presented. The multiple layers of antenna aid in bandwidth enhancement despite the high Q-factor of negative refractive index material responsible for restricting the antenna bandwidth. The antenna presents tuning capability primarily through dimension variation of negative refractive index structure at both layers. The antenna resonance at desired frequencies can be achieved without modifying antenna mechanical dimensions, which aids in surface mountable satellite payload antenna design. The antenna has resonances at 1.57 GHz, 2.48 GHz, and 3.4 GHz frequencies with peak gain at antenna boresight in order of 3.8 dBi, 6.15 dBi, and 4.54 dBi. The proposed multiband antenna offers utilization in the L-band and S-band for satellite and maritime transmit and/or receive operations.

## REFERENCES

1. Veselago, V. G., "Electrodynamics of substances with simultaneously negative  $\epsilon$  and  $\mu$ ," *Usp. Fiz. Nauk.*, Vol. 92, 517, 1967.
2. Pendry, J. B. and D. R. Smith, "Reversing light with negative refraction," *Physics Today*, Vol. 57, 37–43, 2004.
3. Ramakrishna, S. A., "Physics of negative refractive index materials," *Reports on Progress in Physics*, Vol. 68, No. 2, 449, 2005.
4. Krowne, C. M. and Y. Zhang, *Physics of Negative Refraction and Negative Index Materials*, Springer-Verlag Berlin Heidelberg, 2007.
5. Rajkumar, R. and U. K. Kommuri, "A triangular complementary split ring resonator based compact metamaterial antenna for multiband operation," *Wireless Personal Communications*, Vol. 101, No. 2, 1075–1089, 2018.
6. Daniel, R. S., R. Pandeewari, and S. Raghavan, "A compact metamaterial loaded monopole antenna with offset-fed microstrip line for wireless applications," *AEU — International Journal of Electronics and Communications*, Vol. 83, 88–94, 2018.
7. Chaturvedi, D. and S. Raghavan, "A compact metamaterial-inspired antenna for WBAN application," *Wireless Personal Communications*, Vol. 105, No. 4, 1449–1460, 2019.
8. Sahoo, R. and D. Vakula, "Compact metamaterial inspired conformal dual-band antenna loaded with meander lines and fractal shaped inductor for Wi-Fi and WiMAX applications," *IET Microwaves, Antennas & Propagation*, Vol. 13, No. 13, 2349–2359, 2019.
9. Zhao, M., S. Zhu, J. Chen, X. Chen, and A. Zhang, "Broadband metamaterial aperture antenna for coincidence imaging in terahertz band," *IEEE Access*, Vol. 8, 121311–121318, 2020.
10. Ma, Q., C. B. Shi, T. Y. Chen, M. Q. Qi, Y. B. Li, and T. J. Cui, "Broadband metamaterial lens antennas with special properties by controlling both refractive-index distribution and feed directivity," *Journal of Optics*, Vol. 20, No. 4, 045101, 2018.
11. Ren, J., W. Jiang, and S. Gong, "Low RCS and broadband metamaterial-based low-profile antenna using PCM," *IET Microwaves, Antennas & Propagation*, Vol. 12, No. 11, 1793–1798, 2018.
12. Upadhyaya, T. K., S. P. Kosta, R. Jyoti, and M. Palandoken, "Negative refractive index material-inspired 90-deg electrically tilted ultra wideband resonator," *Optical Engineering*, Vol. 53, No. 10, 107104, 2014.
13. Barati, H., M. H. Fakheri, and A. Abdolali, "Experimental demonstration of metamaterial-assisted antenna beam deflection through folded transformation optics," *Journal of Optics*, Vol. 20, No. 8, 085101, 2018.
14. Sehrai, D. A., M. Asif, W. A. Shah, J. Khan, I. Ullah, M. Ibrar, S. Jan, M. Alibakhshikenari, F. Falcone, and E. Limiti, "Metasurface-based wideband MIMO antenna for 5G millimeter-wave systems," *IEEE Access*, 2021.
15. Mark, R., N. Rajak, K. Mandal, and S. Das, "Metamaterial based superstrate towards the isolation and gain enhancement of MIMO antenna for WLAN application," *AEU — International Journal of Electronics and Communications*, Vol. 100, 144–152, 2019.

16. Shabbir, T., R. Saleem, S. S. Al-Bawri, M. F. Shafique, and M. T. Islam, "Eight-port metamaterial loaded UWB-MIMO antenna system for 3D system-in-package applications," *IEEE Access*, Vol. 8, 106982–106992, 2020.
17. Zhu, X., X. Yang, Q. Song, and B. Lui, "Compact UWB-MIMO antenna with metamaterial FSS decoupling structure," *EURASIP Journal on Wireless Communications and Networking*, Vol. 2017, No. 1, 1–6, 2017.
18. Desai, A. and T. Upadhyaya, "Transparent dual band antenna with  $\mu$ -negative material loading for smart devices," *Microwave and Optical Technology Letters*, Vol. 60, No. 11, 2805–2811, 2018.
19. Liu, D., J. Niu, H. Zhu, and J. Zhang, "Ultra-high-frequency microwave response from flexible transparent Au electromagnetic metamaterialnanopatterned antenna," *Nanotechnology*, Vol. 29, No. 6, 06LT01, 2018.
20. Upadhyaya, T. K., S. P. Kosta, R. Jyoti, and M. Palandöken, "Novel stacked  $\mu$ -negative material-loaded antenna for satellite applications," *International Journal of Microwave and Wireless Technologies*, Vol. 8, No. 2, 229–235, 2016.
21. Borazjani, O., M. Naser-Moghadasi, J. Rashed-Mohassel, and R. Sadeghzadeh, "Design and fabrication of a new high gain multilayer negative refractive index metamaterial antenna for X-band applications," *International Journal of RF and Microwave Computer-Aided Engineering*, Vol. 30, No. 9, e22284, 2020.
22. Patel, U. and T. K. Upadhyaya, "Design and analysis of compact  $\mu$ -negative material loaded wideband electrically compact antenna for WLAN/WiMAX applications," *Progress In Electromagnetics Research M*, Vol. 79, 11–22, 2019.
23. Xavier, G. V. R., A. J. R. Serres, E. G. da Costa, A. C. de Oliveira, L. A. M. M. Nobrega, and V. C. de Souza. "Design and application of a metamaterialsuperstrate on a bio-inspired antenna for partial discharge detection through dielectric windows," *Sensors*, Vol. 19, No. 19, 4255, 2019.
24. Ojo, R., M. F. Jamlos, P. J. Soh, M. A. Jamlos, N. Bahari, Y. S. Lee, S. S. Al-Bawri, M. S. Abdul Karim, and K. A. Khairi, "A triangular MIMO array antenna with a double negative metamaterialsuperstrate to enhance bandwidth and gain," *International Journal of RF and Microwave Computer-Aided Engineering*, Vol. 30, No. 8, e22320, 2020.
25. Cheng, C., W. Chen, Y. Lu, F. Ruan, and G. Li, "Large near-field enhancement in terahertz antennas by using hyperbolic Metamaterials with hole arrays," *Applied Sciences*, Vol. 9, No. 12, 2524, 2019.
26. Tang, M. C., Y. Chen, T. Shi, and R. W. Ziolkowski, "Bandwidth-enhanced, compact, near-field resonant parasitic filtennas with sharp out-of-band suppression," *IEEE Antennas and Wireless Propagation Letters*, Vol. 17, No. 8, 1483–1487, 2018.
27. Wan, J., O. Rybin, and S. Shulga, "Far field focusing for a microwave patch antenna with composite substrate," *Results in Physics*, Vol. 8, 971–976, 2018.
28. Baghel, A. K., S. S. Kulkarni, and S. K. Nayak, "Far-field wireless power transfer using GRIN lens metamaterial at GHz frequency," *IEEE Microwave and Wireless Components Letters*, Vol. 29, No. 6, 424–426, 2019.
29. Lum, K. M., C. Laohapensaeng, and C. Free, "A novel traveling-wave feed technique for circularly polarized planar antennas," *IEEE Microwave and Wireless Components Letters*, Vol. 15, No. 3, 180–182, 2005.
30. Dorsey, W. M. and A. I. Zaghloul, "Dual-band, dual-circularly polarised antenna element," *IET Microwaves, Antennas & Propagation*, Vol. 7, No. 4, 283–290, 2013.
31. Liu, D. and B. Gaucher, "A new multiband antenna for WLAN/cellular applications," *IEEE 60th Vehicular Technology Conference, 2004, VTC2004-Fall*, Vol. 1, 243–246, IEEE, September 2004.
32. Long, J. and D. F. Sievenpiper, "A compact broadband dual-polarized patch antenna for satellite communication/navigation applications," *IEEE Antennas and Wireless Propagation Letters*, Vol. 14, 273–276, 2014.